Optimization of Hg(II) adsorption on bio-apatite based materials using CCD-RSM design: characterization and mechanism studies

Mohammad Javad Amiri, Mehdi Bahrami and Farideh Dehkhodaie

ABSTRACT

Bio-apatite based materials were prepared from bovine bone wastes (BBW) by thermal treatments using a direct flame (BBS) and annealing at 500–1,100 °C (BB500–BB1100). These low-crystalline materials were characterized by means of SEM, XRD, FTIR, TG, and pH_{PZC} and were used for the adsorption of Hg(II) ions. A CCD-RSM design was used to optimize and analyze independent variables consisting of initial mercury concentration (10–100 mg L^{-1}), pH (2–9), adsorbent mass (0.1–0.5 g), temperature (20–60 °C), and contact time (15–120 min). The results indicated that the order of the mercury uptakes for bio-apatite based adsorbents was BB500 > BB600 > BB800 > BB1100 > BBS > BBW. The dissolution–precipitation and ion-exchange reaction are the two dominant mechanisms for the removal of Hg(II) ions at low and high pH values, respectively. The CCD-RSM predicted maximum mercury adsorption of 99.99% under the optimal conditions of 51.31 mg L^{-1}, 0.44 g, 6.5, 67.5 min, and 50 °C for initial mercury concentration, adsorbent mass, pH, contact time, and temperature, respectively. The findings of the present study revealed that the bio-apatite based materials, particularly BB500, are suitable and versatile adsorbents for the treatment of mercury-containing wastewater.

Key words | crystalline material, dissolution–precipitation, ion exchange, thermal treatment

Mohammad Javad Amiri (corresponding author)
Mehdi Bahrami
Farideh Dehkhodaie
Department of Water Engineering,
Faculty of Agriculture,
Fasa University,
74616-86131 Fasa,
Iran
E-mail: *mj_amiri@fasau.ac.ir*

INTRODUCTION

In the recent decade, mercury removal has gained much attention due to its serious and dangerous impact on human health and the aquatic environment (Hassan *et al.* 2008; Arshadi *et al.* 2015; Amiri *et al.* 2016; Gil *et al.* 2018). Mercury contamination of the aquatic environment is often caused by the effluents from several industries such as chlor-alkali, agricultural chemicals, fertilizers, paper and pulp, paint, fluorescent lamps, pharmaceuticals, rubber processing, batteries and oil refining (Yardim *et al.* 2003; Hassan *et al.* 2008). A concentration of mercury higher than permissible limits (0.005 mg L^{-1} for wastewater and 0.001 mg L^{-1} for drinking water) defined by the European Union (Di Natale *et al.* 2006) can cause adverse health problems such as neurological damage, chromosome breakage, kidney disease, and pulmonary failure (Hassan *et al.* 2008). When elemental mercury reaches surface waters or soil microorganisms it is oxidized and changed to an organometallic compound named methylmercury ($MeHg,(CH_3Hg^+)X^-$). This substance is extremely toxic and bioaccumulates in fish and shellfish (Yu *et al.* 2016). For example, the consumption of fish containing methylmercury caused a neurological syndrome named Minamata disease in Japan in 1956 (Taty-Costodes *et al.* 2003). Thus, efficient technologies must be used for the elimination of mercury from aquatic media.

Sulfide precipitation, iron coagulation, flocculation, evaporation, ion exchange, membrane separation, and adsorption onto activated carbon have been cited for

doi: 10.2166/wh.2019.039

removal of mercury (Di Natale *et al.* 2006). Among the above-mentioned methods, the biosorption technique has gained a great deal of attention in terms of its simplicity, low cost, and efficiency in removing mercury from dilute solutions (Wang & Chen 2009). Previous studies have indicated that hydroxyapatite (HAP) based materials have a high ability to remove inorganic pollutants from wastewater (Hassan *et al.* 2008; Dimovic *et al.* 2009; Pan *et al.* 2009; Amiri *et al.* 2013a, 2013b; Sljivic-Ivanovic *et al.* 2015). HAP, with the formula $Ca_{10}(PO_4)_6(OH)_2$, has unique properties, such as low solubility, high stability, excellent buffering properties, and high specific surface area, which suggests it is a versatile adsorbent in environmental remediation (Dimovic *et al.* 2009; Sljivic-Ivanovic *et al.* 2015). Bones contain about 70% inorganic phase and 30% organic compounds by weight. The organic compounds consist of the fibrous protein collagen, whereas the inorganic phase comprises poorly crystalline forms of HAP (Dimovic *et al.* 2009). Previous studies indicated that the pristine bone has a low capacity for elimination of heavy metals from aqueous solution due to its collagen and other organic compounds, which can block the suitable active sites of the adsorbent (Kizilkaya *et al.* 2010; Amiri *et al.* 2016, 2018). As a result, a physical (Hassan *et al.* 2008; Dimovic *et al.* 2009; Pan *et al.* 2009; Amiri *et al.* 2013a, 2013b) or chemical (Kizilkaya *et al.* 2010; Amiri *et al.* 2016; Amiri *et al.* 2018) modification has been employed to increase the adsorption capacity and open up the physical structure of bones. Also, bio-apatite based materials can be modified with nanoscale zerovalent iron particles (Amiri *et al.* 2017; Gil *et al.* 2018) or magnetic Fe_3O_4 (Dong *et al.* 2010; Feng *et al.* 2010) to boost the adsorption capacity of adsorbent.

In a classical batch mode experiment, optimization is performed by changing one of the independent parameters while maintaining the other variable fixed ones. This procedure is costly and time-consuming because it requires many experimental runs. Response surface methodology (RSM) based on central composite design (CCD) (CCD-RSM) is a set of statistical techniques and mathematical tools, which can be used for modeling and optimizing processes (Khayet *et al.* 2008). Reducing the number of experiments, considering the interaction effects between parameters, and determining the optimum conditions are the main advantages of RSM (Khayet *et al.* 2008).

The goal of this research was to study the possibility of Hg(II) ions' elimination from simulated wastewater by HAP extracted from bovine bone ash. In this regard, a combination of different operational parameters, such as initial Hg(II) concentration (C_o), pH of the solution, adsorbent dosage (C_s), contact time (t), and solution temperature (T) on removal of Hg(II) ions by adsorption on thermal activated bovine bone waste using CCD-RSM design was adopted from Minitab software Version 16. Finally, optimum conditions of operational parameters for predicting maximum removal efficiency of mercury by HAP were determined.

MATERIALS AND METHODS

Adsorbents

Fresh bovine bone wastes were prepared from a local butcher's shop in Fasa, (Iran). First, bone wastes were cleaned of fat and meat, rinsed with hot water several times, and placed in the open air to eliminate odors. Afterwards, the bones were transferred to an oven at 343 K overnight for drying. Dried bones were crushed and pulverized at between 180 and 355 μm and designated as BBW (see Figure S1, available with the online version of this paper). In order to eliminate the organic components of BBW, an amount of it was burned by using the direct flame of a Bunsen burner until a black material was obtained. The obtained black powder was named bone soot and designated as BBS (see Figure S1). The rest of the BBW was placed in an electric furnace under ambient conditions and set at several temperatures, including 500, 600, 800, and 1,100 °C within 3 hours. These samples were designated as BB500, BB600, BB800, and BB1100 (see Figure S1). As seen in Figure S1, the color of the bio-apatite based materials changed from brown (BBW) to black powder (BBS) and by heat treating gray powder (BB500, BB600, and BB800) was obtained. The gray powder changed to a white powder after further heat treatment (BB1100).

Adsorbate

Mercury(II) sulfate ($HgSO_4$, molecular weight 296.653 g mol^{-1}) was provided by Merck Co., Germany. Working

solutions of mercury were prepared from a stock solution (1,000 mg L^{-1}) by dilution with distilled/deionized water.

Characterization

The equilibrium concentrations of Hg(II) ions in aqueous solution were measured using an atomic absorption spectrophotometer (Perkin-Elmer 3030). The specific surface area of the samples was determined by nitrogen adsorption at −196 °C using Belsorp mini II instruments. A Fourier transform infrared spectrometer (FTIR) (Jasco FT/IR-680 plus spectrophotometer) was used to identify the chemical features of BBW and different thermal activated samples and also to determine their various functional groups before and after contact with Hg(II) ions. The spectra of the samples were recorded in the range of 4,000–400 cm^{-1} using KBr pellets. In order to determine the composition and morphology of the samples, a scanning electron microscope (SEM) (VEGA3 TESCAN) was used. The chemical composition of the samples was determined using energy-dispersive X-ray (EDX). A Philips X'PERT MPD diffractometer was employed to investigate the crystalline features of the samples. The X-ray diffraction (XRD) pattern was obtained at 40 kV and 30 mA in the 2θ range of 10–100°. Mass loss pattern of BBW during heating was measured by thermogravimetric analysis (TGA) (Setaram TG-DTA92). A zeta potential meter (Zetasizer nano-ZS90 Malvern) and a pH/mV meter (Metrohm, 827 pH Lab) were used to determine the point of zero charges (pH_{PZC}) of the samples and to measure the pH of the solutions, respectively.

Adsorption experiments

Batch experiments were performed to study the adsorption performance of Hg(II) ions onto bio-apatite based materials. In this regard, different amounts of bio-apatite materials (0.1–0.5 g) were shaken with 100 mL of the Hg(II) solution, ranging between 10 and 100 mg L^{-1} at several temperatures (20–60 C) and contact times (15–120 min). Also, the pH of solutions was adjusted in the range of 2–9 by adding 0.1 M NaOH/HCl. After shaking for the required time, the solutions were filtered through filter paper (Whatman grade 40) and analyzed by using an atomic absorption spectrophotometer. The removal efficiency of Hg(II) ions at equilibrium was calculated by the following equation:

$$R = \frac{C_o - C_e}{C_o} \quad (1)$$

where R is the adsorption efficiency (%) of Hg(II) ions by different bone samples, C_0 is the initial Hg(II) concentration of the solution (mg L^{-1}), and C_e is the residual Hg(II) concentration of the solution (mg L^{-1}).

CCD-RSM

In this research, RSM coupled with a CCD matrix (CCD-RSM) was employed for the following purposes: (1) reduce the number of experiments; (2) analyze the interaction effects between operating parameters; (3) determine the optimum conditions of operating parameters; and (4) fit the second-order polynomial equation to predict the removal efficiency of Hg(II) ions. Five independent variables consisting of initial Hg(II) concentration (C_o), pH of the solution, adsorbent dosage (C_s), contact time (t), and solution temperature (T) were considered as the input of CCD-RSM and the removal efficiency of Hg(II) ions as the output. The design was formed at five levels (very low, low, medium, high, and very high) and a total of 54 experiments were performed. The ranges of the five independent factors and 54 experiments, including removal efficiency of Hg(II) ions and their operating parameters for each bio-apatite based material, are presented in Tables S1 and S2, respectively (available online). These 54 runs include 32 factorial runs, 16 axial runs, and six center runs. In this work, α, which is defined as the distance of the axial point from the center, is equal to 2.37. The amount of α was obtained by the following equation (Zhu *et al.* 2017):

$$\alpha = 2^{\frac{n}{4}} \quad (2)$$

where n is the number of independent factors and is equal to 5 in this study. In order to perform the statistical analyses, the real amounts of independent variables, (X_i, $i = 1, 2, 3, 4$ and 5) including (Co (X_1), Cs (X_2),

t (X_3), pH (X_4), and T (X_5)), were transformed into a coded value (x_i) by the following equation:

$$x_i = \frac{X_i - X_0}{\Delta X} \tag{3}$$

where X_o and ΔX are the real value of the independent factor at the central point and the step size, respectively. In the CCD-RSM model, the experimental data were fitted into the second-order polynomial equation by regression analysis (Zhu *et al.* 2017).

$$y = b_0 + \sum_{i=1}^{k} b_i x_i + \sum_{i=1}^{k} b_{ii} x_{ii}^2 + \sum_{i=1}^{k} \sum_{j=i+1}^{k} b_{ij} x_i x_j + \varepsilon \tag{4}$$

where y is the estimated removal percentage of Hg(II) ions (%), x_i and x_j are the coded independent factors (C_o, Cs, t, pH, and T), which were run, b_0 is a constant coefficient and b_i, b_{ii}, and b_{ij} are the linear, quadratic, and interaction effect regression coefficients, respectively (i = 1, 2, 3, 4, and 5), ε is the statistical error and k is the number of the patterns. These regression coefficients can be determined using the ordinary least squares method as follows:

$$b = (X^T X)^{-1} X^T Y \tag{5}$$

where b and Y are the vector of regression coefficients and response, respectively. Also, X is a matrix of the coded levels of operating parameters.

RESULTS AND DISCUSSION

Characterization of the bio-apatite based adsorbents

The FTIR spectrum of the bio-apatite based materials was recorded in the range of 4,000–400 cm^{-1} (see Figure 1). The FTIR analysis of bio-apatite based materials demonstrates the presence of the phosphate and carbonate groups, which is from HAP, and the organic components such as amide functional groups (Boskey & Camacho 2007). The inorganic components are divided into three main groups, carbonate, phosphate, and hydroxyl, and all of them have been observed in the FTIR spectrum of bio-apatite based materials (Bahrololoom *et al.* 2009). The bands observed at 1,091, 1,035, 962, 603, and 570 cm^{-1} are ascribed to various modes of PO_4^{-3} in all the bio-apatite based materials (see Figure 1) (Dimovic *et al.* 2009; Amiri *et al.* 2016). The broad band in the spectra of BBW and a small band in the spectra of BBS, BB500, BB600, BB800, and BB1100 at about 3,500 and 3,400 cm^{-1} are due to the vibrations of hydroxyl groups. Furthermore, a small peak at 3,571 cm^{-1} in the spectra of BB500, BB600, BB800, and BB1100 is related to the carboxyl stretching (Bahrololoom *et al.* 2009). The bands of the carbonate groups were identified at 1,456, 1,415, 871, and 680 cm^{-1} (Bahrololoom *et al.* 2009). The bands at around 2,929 and 2,860 cm^{-1} in the spectra of BBW are due to stretching vibration of the CH_2 and CH_3 (Amiri *et al.* 2018). The bands associated with the C-H groups which are detected in the spectra of BBW are very small and weak for other bio-apatite based materials. This can be related to eliminating organic components after burning bone wastes. The peaks at 1,650, 1,552, and 1,232 cm^{-1} in the spectra of BBW are due to organic components, which are not found in the FTIR spectra of BB500, BB600, BB800, and BB1100. Although this band exists in the FTIR spectra of BBS, it is weaker than the BBW. Unlike the BBW, there is no peak at 1,744 cm^{-1} associated with carbonyl groups in the FTIR spectra of the BBS, BB500, BB600, BB800, and BB1100 (Haberko *et al.* 2006). This demonstrates that thermal treatment is a suitable method to remove organic components from the structure of the bone.

SEM micrographs of the bio-apatite based materials are presented in Figure 2. BBW has a rough surface without visible cracks. The BBS surface with apparent cracks is more irregular than the BBW due to removal of some organic compounds from the structure of bone. Clearly, there is some difference between bio-apatite based materials at various thermal treatments. The surface morphology of BB500 becomes rougher with rising temperature and a porous internal structure is also observed, which can be related to removing organic components from the structure of the bone. At higher heating temperatures ($T > 600\,^{\circ}C$), the pores of bio-apatite based materials were decreased due to an increase of HAP crystallite size (Dimovic *et al.* 2009).

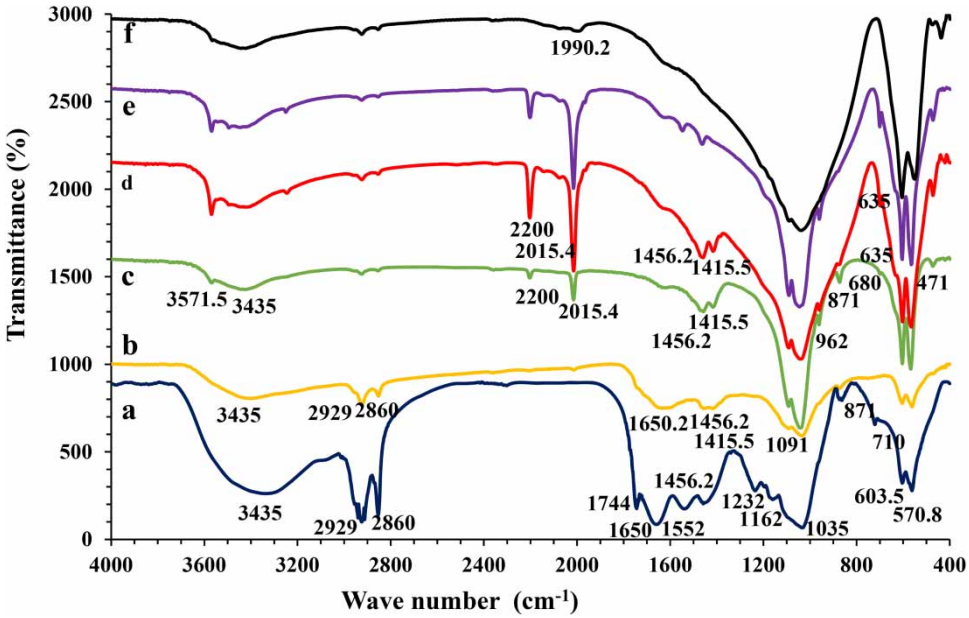

Figure 1 | FTIR spectra of the bio-apatite based materials: (a) BBW, (b) BBS, (c) BB500, (d) BB600, (e) BB800, and (f) BB1100.

TG analysis of the BBW was performed under Ar atmosphere, from 25 to 800 °C with an increasing temperature rate of 10 °C/min (see Figure S2, available with the online version of this paper). As can be seen from Figure S2, the weight loss of BBW can be divided into three main stages, including stage I (81.9–231 °C), stage II (231–494.5 °C), and stage III (494–800 °C) (Deydier *et al.* 2005). Stages I, II, and III are associated with desorption of physically held water, degradation of organic components, and oxidation of CO_3^{-2} from the framework of BBW to CO_2, respectively (Deydier *et al.* 2005).

The specific surface areas of BBW, BBS, BB500, BB600, BB800, and BB1100 were 3, 5, 75, 64, 10, and 5 $m^2\ g^{-1}$, respectively. In fact, by thermal treating up to 500 °C, a significant increase in specific surface area occurs, which can be related to removing organic compounds from the framework of the bone. At higher temperatures ($T > 500$ °C), a decrease in specific surface area was observed, due to an increase of HAP crystallite size (Dimovic *et al.* 2009). These results confirm the previous discussion regarding the influence of the thermal treatment on the bio-apatite based materials by SEM. The pH_{PZC} of BBW, BBS, BB500, BB600, BB800, and BB1100 was 7.8, 7.5, 6.8, 7.1, 10.2, and 10.8, respectively. Among the bio-apatite based materials, BB500 has the most negative surface, which can be suitable for electrostatic interaction between the negative surface of BB500 and the mercury cations.

The XRD patterns of the bio-apatite based materials are presented in Figure S3 (available online). The XRD pattern of the BBW is very broad, which demonstrates the presence of organic compounds and also small crystals of HAP (Wang *et al.* 2010; Amiri *et al.* 2016). An increase in the degree of sharpness of peaks for other bio-apatite based materials appeared due to the removal of organic components and the increase of HAP crystal size (Bahrololoom *et al.* 2009). The results confirm that the HAP peaks become higher in intensity after heat treatment temperature, which was characterized at 2θ at 26, 32, 39, 50, 52, and 64°.

CCD-RSM plots and interaction effect analysis

Three-dimensional surface and contour plots were drawn in order to evaluate the combined effects of two test factors on the adsorption efficiency when the other three factors were retained at their optimum levels. The interaction between pH and initial Hg(II) concentration when the other three factors were fixed is presented in Figure 3. The removal efficiency of Hg(II) ions clearly increased with increasing pH and decreasing initial metal concentration. Similar behavior has been reported for the adsorption of Hg(II) ions onto

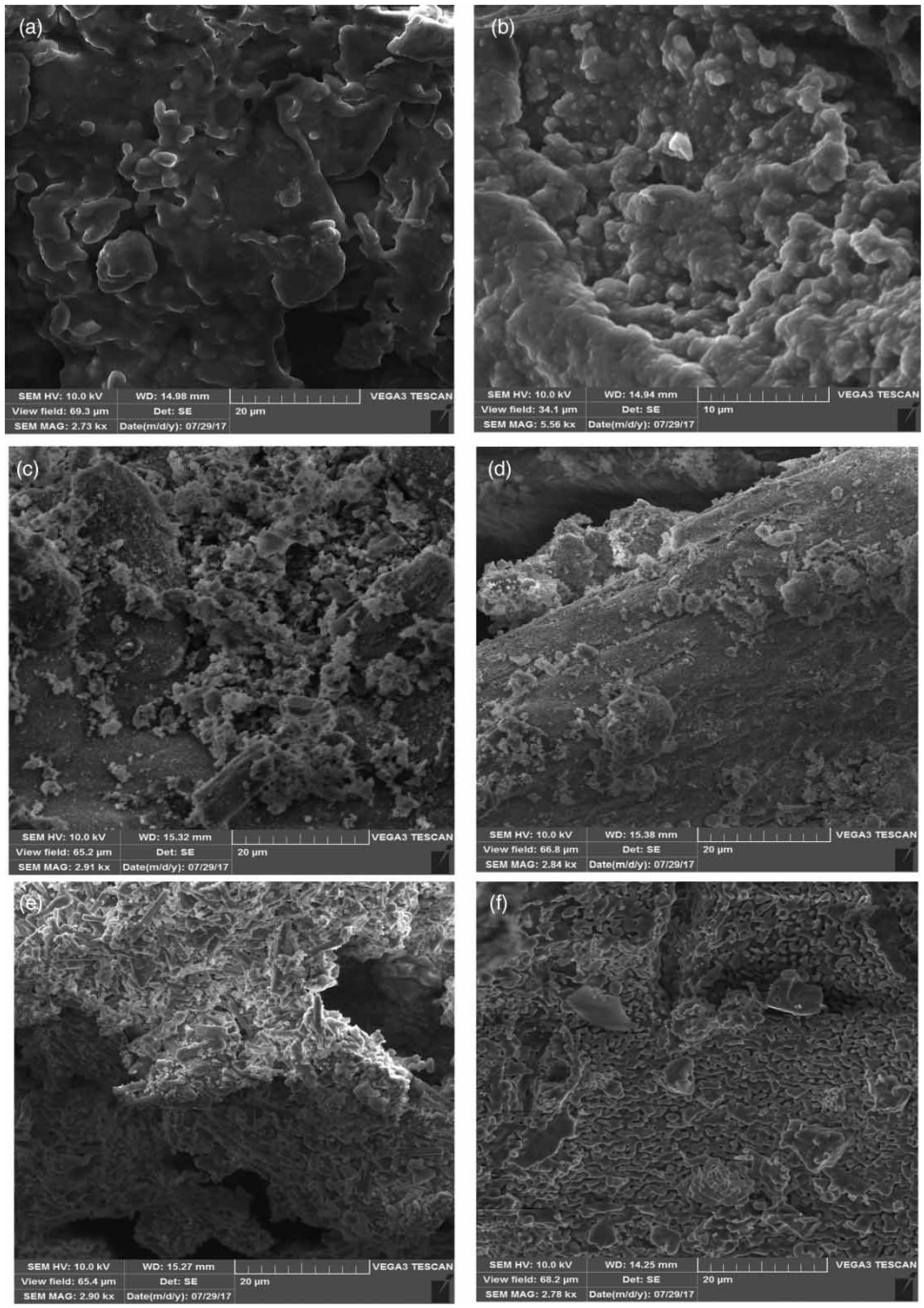

Figure 2 | SEM images of the bio-apatite based materials: (a) BBW, (b) BBS, (c) BB500, (d) BB600, (e) BB800, and (f) BB1100.

bio-apatite based materials (Hassan *et al.* 2008; Amiri *et al.* 2016, 2018). It was found that when the range of initial Hg(II) concentration was between 10 and 100 mg L^{-1}, removal efficiency was between 30 and 40% for BBW and BBS and also 40–60% for BB1100 up to pH 4, but at pH = 5–9, the amounts were in the range of 40 to 50% for BBW and BBS and were >70% for BB1100. Also, as initial Hg(II) concentration range changes from 10 to 100 mg L^{-1}, removal efficiency was between 80 and 90% for BB500, BB600, and BB800 up to pH = 4, but at higher pH, the

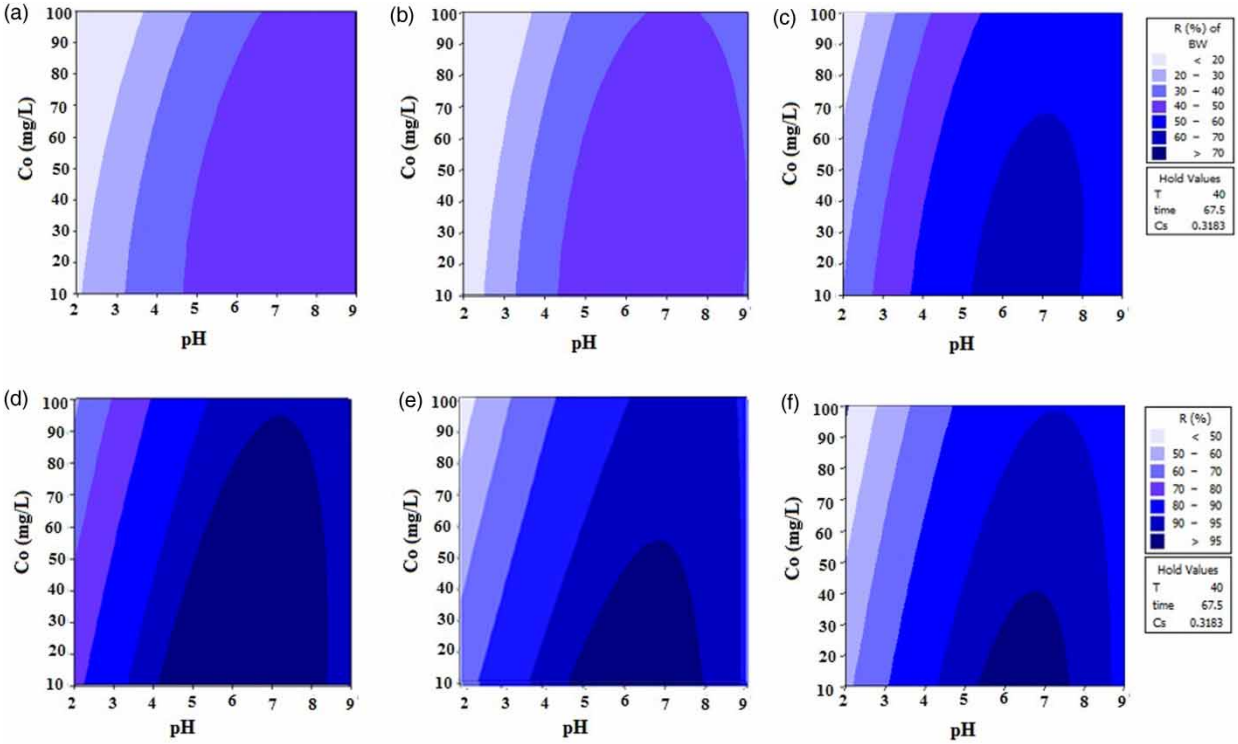

Figure 3 | Contour plots for interaction of C_o * pH: (a) BBW, (b) BBS, (c) BB1100, (d) BB500, (e) BB600, and (f) BB800.

amounts were >90%. Mercury species in the aqueous solution are Hg^{2+}, $Hg(OH)^{+}$, and $Hg(OH)_2$ at different pH (Amiri *et al.* 2017). At low pH (pH < 4), a high concentration of hydrogen ions compete with cationic species of mercury for binding to active sites, thus resulting in lower removal efficiency of Hg(II). Furthermore, electrostatic repulsion between the cationic species of mercury and the positive charge of bio-apatite based materials may occur. At pH between 4 and 8, bio-apatite based materials gain deprotonation and Hg(II) ions are favorably adsorbed on the surface of the adsorbent. At pH >7, the removal of Hg(II) ions was performed by both adsorption and precipitation reactions due to the precipitation of $Hg(OH)_2$. Although the adsorption of Hg(II) ions decreased in the pH range between 8 and 9, which can be explained by the fact that the mobility of mercury and consequently the exchangeable form of it decreased, it resulted in a decrease in the contact probability between bio-apatite based materials and Hg(II) ions. In addition, a high concentration of OH^{-} ions competes with cationic species of mercury for binding to active sites, thereby, adsorption of Hg(II) was reduced. A high adsorption efficiency of Hg(II) ions at $pH < pH_{PZC}$ for all bio-apatite based adsorbents indicates that the electrostatic attractions are not the predominant mechanism in Hg(II) removal. Thus, the degree of ionization, surface charge of the bio-apatite based materials, and speciation of mercury are affected by the initial pH of the solution.

Figure 4 illustrates the surface plots of bio-apatite based materials for the interaction of initial pH with contact time when other factors were kept constant. In all bio-apatite based adsorbents, the adsorption process of mercury was fast and equilibrium time was attained at nearly 15–20 min. The results indicated that the BB500 had the best performance to remove Hg(II) ions from aqueous solution by opening up the physical structure of the BBW to grant more active sites. Figure 5 shows the contour plots of adsorption efficiency as a function of pH and temperature when the other factors were fixed. As seen, the removal efficiency of Hg(II) ions by all bio-apatite based materials ions was increased with rising temperature, confirming the endothermic nature of the adsorption processes. This trend can be related to activation of the sorption surface and enlarging

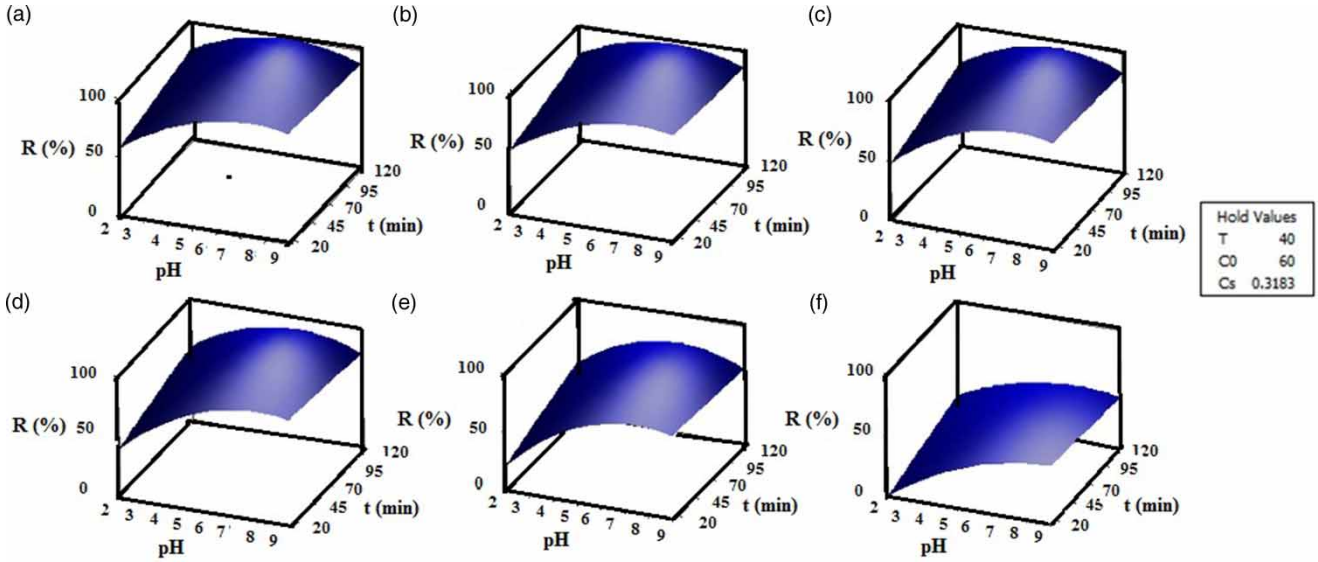

Figure 4 | Surface plots for interaction of t * pH: (a) BB500, (b) BB600, (c) BB800, (d) BB1100, (e) BBS and (f) BBW.

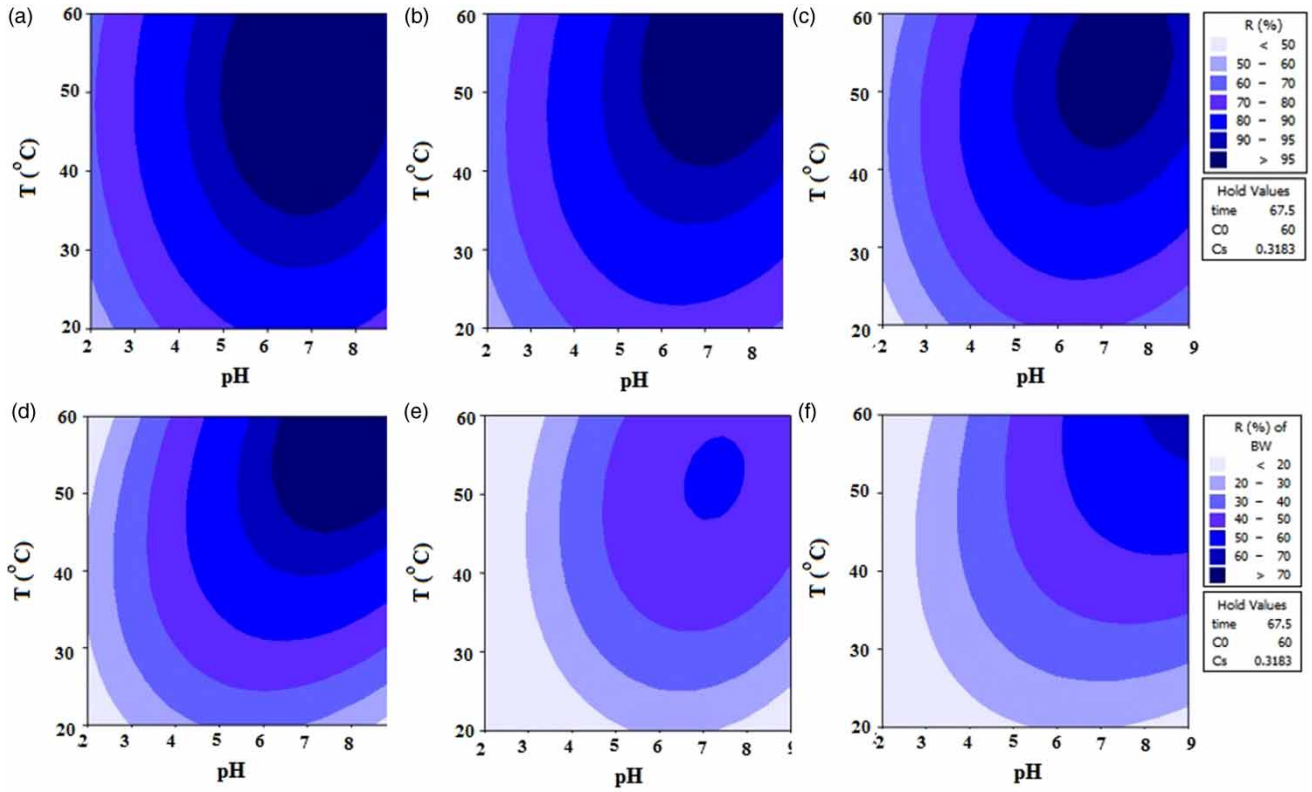

Figure 5 | Contour plots for interaction of T * pH: (a) BB500, (b) BB600, (c) BB800, (d) BB1100, (e) BBS, and (f) BBW.

the pore size (Srivastava *et al.* 2015), thereby, the diffusion of mercury ions into the bio-apatite pores was increased (Amiri *et al.* 2016). Also, precipitation of the mercury hydroxide happens quickly at high temperatures (Javanbakht & Ghoreishi 2017). Figure 6 indicates the combined effect of adsorbent dosage and initial Hg(II) concentration on

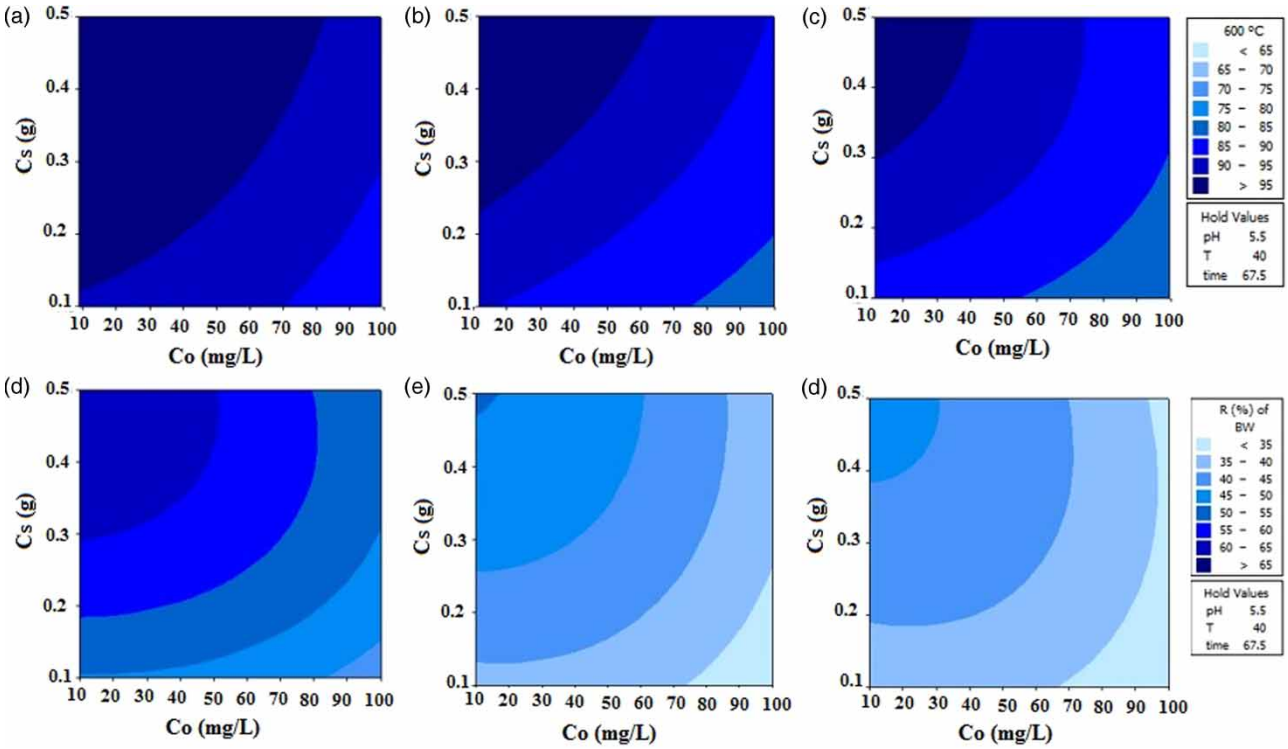

Figure 6 | Contour plots for interaction of C_o * C_s: (a) BB500, (b) BB600, (c) BB800, (d) BB1100, (e) BBS, and (f) BBW.

adsorption efficiency at the constant other three factors. It is clear that the adsorption efficiency was increased with a decrease in initial metal concentration from 10 to 100 mg L^{-1} and an increase in adsorbent mass from 0.1 to 0.5 g. Maximum percentage removal of mercury was achieved at a minimum initial concentration (10 mg L^{-1}), which was due to the sufficient available active sites and, consequently, more surface area. Based on the contour plots, the order of the mercury uptake for bio-apatite based adsorbents was BB500 > BB600 > BB800 > BB1100 > BBS > BBW (see Figures 3–6). This trend is according to the BET surface area of samples. Similar results were reported by Dimovic *et al.* (2009) and Cazetta *et al.* (2014).

Fitting the model

The regression equations based on the second-order polynomial model between the removal efficiency of Hg(II) ions and the five independent factors (initial Hg(II) concentration (C_o), pH of the solution, adsorbent dosage (C_s), contact time (t), and solution temperature (T)) are presented in Table 1. In these equations, the negative and positive signs in front of the factors demonstrate antagonistic and synergistic effects, respectively. The determination coefficient (R^2) was employed to determine the accuracy of the equations. The R^2 of BBW, BBS, BB500, BB600, BB800, and BB1100 was 0.953, 0.926, 0.947, 0.943, 0.967, and 0.898, respectively. Also, R^2_{adj} of BBW, BBS, BB500, BB600, BB800, and BB1100 was 0.949, 0.918, 0.938, 0.937, 0.955, and 0.889, respectively. The high values of R^2 and R^2_{adj} for different bio-apatite adsorbents indicate that this model can describe the experimental data well. The predicted R^2 (R^2_{pred}) of BBW, BBS, BB500, BB600, BB800, and BB1100 was 0.902, 0.8844, 0.919, 0.912, 0.897, and 0.853, respectively. The R^2_{pred} is also high, which displays good reliability to predict removal efficiency of Hg(II) ions. The sensitivity of the CCD-RSM to five independent factors is conducted by analysis of variance (ANOVA). This analysis indicates that an independent variable with a larger F value and a lower p value has a more significant influence on the removal efficiency of Hg(II) ions. Table S3 (available online) implies that the removal efficiency of Hg(II) ions is more sensitive

Table 1 | The second-order polynomial equation for bio-apatite based materials

RBBW $= -74.29 + 12.64pH + 1.615T + 0.17t - 0.058C_o + 103.98C_s - 0.962pH^2 - 0.021T^2 - 0.001C_o^2 - 51.94C_s^2 + 0.168(pH*T) - 0.036(pH*t) + 0.025(pH*C_o) - 8.54(pH*C_s) - 0.001(T*t) - 0.002(T*C_o) - 0.0174(T*C_s) + 0.002(t*C_o) + 0.11(t*C_s) - 0.187(C_o*C_s)$
RBBS $= -103.87 + 25.67pH + 2.67T + 0.223t - 0.106C_o + 143.09C_s - 1.74pH^2 - 0.03T^2 - 0.001C_o^2 - 49.43C_s^2 + 0.101(pH*T) - 0.042(pH*t) + 0.022(pH*C_o) - 12.95(pH*C_s) - 0.002(T*C_o) - 0.376(T*C_s) + 0.002(t*C_o) + 0.062(t*C_s) - 0.166(C_o*C_s)$
RBB500 $= -36.79 + 20.32pH + 2.11T + 0.115t - 0.0918C_o + 89.71C_s - 1.31pH^2 - 0.186T^2 + 0.0001t^2 - 0.0004C_o^2 - 13.58C_s^2 + 0.0218(pH*T) - 0.034(pH*t) + 0.0296(pH*C_o) - 8.65(pH*C_s) - 0.0005(T*t) - 0.0048(T*C_o) - 0.357(T*C_s) + 0.0014(t*C_o) + 0.0851(t*C_s) - 0.117(C_o*C_s)$
RBB600 $= -34.29 + 18.53pH + 1.88T + 0.025t - 0.139C_o + 126.55C_s - 1.25pH^2 - 0.019T^2 - 20.142C_s^2 - + 0.084(pH*T) - 0.034(pH*t) + 0.033(pH*C_o) - 13.35(pH*C_s) - 0.001(T*C_o) - 0.53(T*C_s) + 0.001(t*C_o) + 0.169(t*C_s) - 0.135(C_o*C_s)$
RBB800 $= -56.37 + 20.72pH + 2.39T + 0.104t - 0.073C_o + 112.35C_s - 1.47pH^2 - 0.025T^2 - 45.78C_s^2 - + 0.084(pH*T) - 0.034(pH*t) + 0.027(pH*C_o) - 9.26(pH*C_s) - 0.005(T*C_o) - 0.336(T*C_s) + 0.001(t*C_o) + 0.12(t*C_s) - 0.157(C_o*C_s)$
RBB1100 $= -76.43 + 20.04pH + 2.26T + 0.141t - 0.007C_o + 189.59C_s - 1.55pH^2 - 0.03T^2 - 0.01C_o^2 - 86.192C_s^2 - + 0.203(pH*T) - 0.041(pH*t) + 0.029(pH*C_o) - 16.38(pH*C_s) - 0.002(T*t) - 0.421(T*C_s) - 0.005(T*C_o) + 0.001(t*C_o) + 0.117(t*C_s) - 0.189(C_o*C_s)$

to the adsorbent dosage, followed by pH, temperature, reaction time, and initial metal concentration (see Table S3).

Optimization of parameters

Optimization of independent input factors for maximizing adsorption efficiency was studied by CCD-RSM and the results are presented in Table 2. The predicted maximum adsorption efficiency of different adsorbents under optimum independent factors (C_o, pH, C_s, t, and T), as calculated by CCD-RSM, has been compared with experimentally determined percentage removal under optimum conditions (see Table 2). For instance, experimentally determined percentage removal of BB500 under the optimal conditions (initial Hg(II) concentration of 51.31 mg L^{-1}, temperature of 50 °C, pH of 6.5, adsorbent mass of 0.44 g, and contact time of 67.5 min) was 97.1%, which was very close to the predicted maximum adsorption efficiency by the model (99.99%).

Mechanism

Two main mechanisms for the adsorption of Hg(II) ions by bio-apatite based materials have been suggested and are dependent upon the pH values (Jang *et al.* 2008). At low pH, the dissolution–precipitation mechanism is dominant, whereas the ion-exchange reaction is dominant at high pH, and is shown as follows (see Figures S4 and S5, available online):

$$\textit{Dissolution}:\ Ca_{10}(PO_4)_6(OH)_2 + 14H^+ \rightarrow 10Ca^{2+} + 6H_2PO_4^- + 2H_2O$$

$$\textit{Precipitation}:\ 10Hg^{2+} + 6H_2PO_4^- + 2H_2O \rightarrow 14H^+ + Hg_{10}(PO_4)_6(OH)_2$$

$$\textit{Ion exchange}:\ Ca_{10}(PO_4)_6(OH)_2 + xHg^+ \rightarrow xCa^{2+} + Ca_{10-x}Hg_x(PO_4)_6(OH)_2$$

At low pH, the dissolution of $Ca_{10}(PO_4)_6(OH)_2$ in the aqueous solution comprising Hg(II) is followed by

Table 2 | Optimization of independent input factors for different bio-apatite based materials

Independent input parameters	BBW	BBS	BB500	BB600	BB800	BB1100
Initial Hg(II) concentration (mg L^{-1})	12.68	12.68	51.31	32.39	12.68	12.68
Adsorbent mass (g)	0.44	0.48	0.44	0.44	0.44	0.44
pH	9	7.2	6.5	6.5	6.5	7
Contact time (min)	14.26	14.26	67.5	67.5	103.97	120
Temperature (°C)	56.1	53.2	50	50	50	55.66
Actual removal efficiency	55.1	76.66	97.1	93.65	89.88	85.61
Predicted removal efficiency	60.33	81.88	99.99	99.99	94.99	88.99

precipitation of $Hg_{10}(PO_4)_6(OH)_2$. The adsorption of Hg(II) ions onto the bio-apatite based materials' surface occurred following ion-exchange reaction between Hg(II) ions in solution and Ca^{2+} ions of $Ca_{10}(PO_4)_6(OH)_2$. The details are provided in the Supplementary data (available with the online version of this paper).

Kinetic and isotherm studies

The kinetics of mercury uptake onto bio-apatite based materials was assessed with the pseudo first-order and pseudo second-order models. Also, isotherm models have been investigated in terms of Langmuir, Freundlich, and Langmuir–Freundlich equations. These models and associated parameters are presented in Table S4. Mathematical models were evaluated by comparing the coefficient of determination (R^2). The kinetic data of bio-apatite based materials were described well by the pseudo second-order model ($R^2 >$ 0.97), which shows the rate-limiting step for the capturing of mercury on bio-apatite materials is chemisorption and confirms the proposed mechanism (see Table S5). BB500 had the highest rate constant (k_2), whereas the lowest value was observed for BBW. The isotherm modeling showed that the Langmuir–Freundlich model characterizes the equilibrium sorption data satisfactorily (see Table S6). The estimated maximum uptake capacities using the Langmuir–Freundlich model for BB500, BB600, BB800, BB1100, BBS, and BBW were 78.5, 70.7, 66.1, 43.7, 35.4, and 21.2 mg g^{-1}, respectively (see Table S6), which confirms the results of the contour plots of Figures 3–6. (Tables S4–S6 are available online.)

CONCLUSION

Extraction of bio-apatite based materials from bovine bone wastes through thermal treatments produces versatile and valuable adsorbents for the removal of Hg(II) ions from wastewater. The effects of the five independent factors (pH, initial metal concentration, adsorbent dosage, temperature, and contact time) were considered for the percentage removal of mercury according to the CCD-RSM design. Characterization of the bio-apatite based adsorbents demonstrated that the thermal treatment is an efficient method to remove organic compounds from the framework of bone. The order of mercury removal by different bio-apatite based materials was: BB500 > BB600 > BB800 > BB1100 > BBS > BBW, which demonstrated that heating at 500 °C was the optimal treatment for immobilization of Hg(II) ions. According to the attained results, burning the BBW at higher heating temperatures, particularly above 600 °C, led to reducing the specific surface area and, consequently, removal efficiency. The highest single and interaction effects of the five independent factors were observed for adsorbent dosage and adsorbent dosage versus pH, respectively. From a practical point of view, the bio-apatite based materials can be used as suitable adsorbents for the treatment of mercury-containing wastewater.

REFERENCES

Amiri, M. J., Abedi-Koupai, J., Eslamian, S. S., Mousavi, S. F. & Arshadi, M. 2013a Modelling Pb(II) adsorption based on synthetic and industrial wastewaters by ostrich bone char using artificial neural network and multivariate non-linear regression. *Int. J. Hydrol. Sci. Technol.* **3** (3), 221–240.

Amiri, M. J., Abedi-Koupai, J., Eslamian, S. S., Mousavi, S. F. & Hasheminejad, H. 2013b Modeling Pb(II) adsorption from aqueous solution by ostrich bone ash using adaptive neural-based fuzzy inference system. *J. Environ. Sci. Health Part A* **48** (5), 543–558.

Amiri, M. J., Abedi-Koupai, J., Eslamian, S. S. & Arshadi, M. 2016 Adsorption of Pb(II) and Hg(II) ions from aqueous single metal solutions by using surfactant-modified ostrich bone waste. *Desalin. Water Treat.* **57**, 16522–16539.

Amiri, M. J., Abedi-koupai, J. & Eslamian, S. 2017 Adsorption of Hg(II) and Pb(II) ions by nanoscale zero-valent iron supported on ostrich bone ash in a fixed-bed column system. *Water Sci. Technol.* **76** (3), 671–682.

Amiri, M. J., Arshadi, M., Giannakopoulos, E. & Kalavrouziotis, I. K. 2018 Removal of mercury (II) and lead (II) from aqueous media by using a green adsorbent: kinetics, thermodynamic, and mechanism studies. *J. Hazard. Toxic Radioact. Waste* **22** (2), 04017026.

Arshadi, M., Faraji, A. R. & Amiri, M. J. 2015 Modification of aluminum–silicate nanoparticles by melamine-based dendrimer L-cysteine methyl esters for adsorptive characteristic of Hg(II) ions from the synthetic and Persian Gulf water. *Chem. Eng. J.* **266**, 345–355.

Bahrololoom, M. E., Javidi, M., Javadpour, S. & Ma, J. 2009 Characterization of natural hydroxyapatite extracted from bovine cortical bone ash. *J. Ceram. Process. Res.* **10** (2), 129–138.

Boskey, A. & Camacho, N. P. 2007 FT-IR imaging of native and tissue-engineered bone and cartilage. *Biomaterials* **28** (15), 2465–2478.

Cazetta, A. L., Azevedo, S. P., Pezoti, O., Souza, L. S., Vargas, A. M. M., Paulino, A. T., Moraes, J. C. G. & Almeida, V. C. 2014 Thermally activated carbon from bovine bone: optimization of synthesis conditions by response surface methodology. *J. Anal. Appl. Pyrolysis* **110**, 455–462.

Deydier, E., Guilet, R., Sarda, S. & Sharrock, P. 2005 Physical and chemical characterisation of crude meat and bone meal combustion residue: 'waste or raw material?'. *J. Hazard. Mater.* **121**, 141–148.

Dimovic, S., Smiciklas, I., Plecas, I., Antonovic, D. & Mitric, M. 2009 Comparative study of differently treated animal bones for Co^{2+} removal. *J. Hazard. Mater.* **164**, 279–287.

Di Natale, F., Lancia, A., Molino, A., Di Natale, M., Karatza, D. & Musmarra, D. 2006 Capture of mercury ions by natural and industrial materials. *J. Hazard. Mater.* **132**, 220–225.

Dong, L., Zhu, Z., Qiu, Y. & Zhao, J. 2010 Removal of lead from aqueous solution by hydroxyapatite/magnetite composite adsorbent. *Chem. Eng. J.* **165** (3), 827–834.

Feng, Y., Gong, J. L., Zeng, G. M., Niu, Q. Y., Zhang, H. Y., Niu, C. G., Deng, J. H. & Yan, M. 2010 Adsorption of Cd (II) and Zn (II) from aqueous solutions using magnetic hydroxyapatite nanoparticles as adsorbents. *Chem. Eng. J.* **162** (2), 487–494.

Gil, A., Amiri, M. J., Abedi-Koupai, J. & Eslamian, S. 2018 Adsorption/reduction of Hg (II) and Pb (II) from aqueous solutions by using bone ash/nZVI composite: effects of aging time, Fe loading quantity and co-existing ions. *Environ. Sci. Pollut. Res.* **25**, 2814–2829.

Haberko, K., Bucko, M. M., Brzezinska-Miecznik, J., Haberko, M., Mozgawa, W., Panz, T., Pyda, A. & Zarebski, J. 2006 Natural hydroxyapatite – its behavior during heat treatment. *J. Eur. Ceram. Soc.* **26**, 537–542.

Hassan, S. S. M., Awwad, N. S. & Aboterika, A. H. A. 2008 Removal of mercury (II) from wastewater using camel bone charcoal. *J. Hazard. Mater.* **154** (1–3), 992–997.

Jang, S. H., Min, B. G., Jeong, Y. G., Lyoo, W. S. & Lee, S. C. 2008 Removal of lead ions in aqueous solution by hydroxyapatite/polyurethane composite foams. *J. Hazard. Mater.* **152**, 1285–1292.

Javanbakht, V. & Ghoreishi, S. M. 2017 Application of response surface methodology for optimization of lead removal from an aqueous solution by a novel superparamagnetic nanocomposite. *Adsorp. Sci. Technol.* **35** (1–2), 241–260.

Khayet, M., Cojocarub, C. & Zakrzewska-Trznadelc, G. 2008 Response surface modelling and optimization in pervaporation. *J. Membrane Sci.* **321**, 272–283.

Kizilkaya, B., Tekinary, A. A. & Dilgin, Y. 2010 Adsorption and removal of Cu (II) ions from aqueous solution using pretreated fish bones. *Desalination* **264**, 37–47.

Pan, X., Wang, J. & Zhang, D. 2009 Sorption of cobalt to bone char: kinetics, competitive sorption and mechanism. *Desalination* **249** (2), 609–614.

Sljivic-Ivanovic, M., Smiciklas, I., Milenkovic, A., Dojcinovic, B., Babic, B. & Mitric, M. 2015 Evaluation of the effects of treatment factors on the properties of bio-apatite materials. *J. Mater. Sci.* **50**, 354–365.

Srivastava, V., Sharma, Y. C. & Sillanpaa, M. 2015 Response surface methodological approach for the optimization of adsorption process in the removal of Cr(VI) ions by $Cu_2(OH)_2CO_3$ nanoparticles. *Appl. Surf. Sci.* **326**, 257–270.

Taty-Costodes, V. C., Fauduet, H., Porte, C. & Delacroix, A. 2003 Removal of Cd(II) and Pb(II) ions, from aqueous solutions, by adsorption onto sawdust of *Pinus sylvestris*. *J. Hazard. Mater.* **B105**, 121–142.

Wang, J. & Chen, C. 2009 Biosorbents for heavy metals removal and their future. *Biotechnol. Adv.* **27** (2), 195–226.

Wang, X. Y., Zuo, Y., Huang, D., Hou, X. D. & Li, Y. B. 2010 Comparative study on inorganic composition and crystallographic properties of cortical and cancellous bone. *Biomed. Environ. Sci.* **23**, 473–480.

Yardim, M. F., Budinova, T., Ekinci, E., Petrov, N., Razvigorova, M. & Minkova, V. 2003 Removal of mercury (II) from aqueous solution by activated carbon obtained from furfural. *Chemosphere* **52**, 835–841.

Yu, J.-G., Yue, B.-Y., Wu, X.-W., Liu, Q., Jiao, F.-P., Jiang, X.-Y. & Chen, X.-Q. 2016 Removal of mercury by adsorption: a review. *Environ. Sci. Pollut. Res.* **23** (6), 5056–5076.

Zhu, M., Yao, J., Qin, Z., Lian, L. & Zhang, C. 2017 Response surface methodology approach for the optimisation of adsorption of hydrolysed polyacrylamide from polymer-flooding wastewater onto steel slag: a good option of waste mitigation. *Water Sci. Technol.* **76** (3–4), 776–784.

First received 15 February 2019; accepted in revised form 24 March 2019. Available online 19 April 2019